Estimating the Spatial Resolution of fNIRS Sensors for BCI Purposes

Rand Kasim Almajidy *[a, b, c], Robert D. Kirch [a], Olaf Christ [a], Ulrich G. Hofmann [a]

[a] Neuroelectronic Systems, Dept. of Neurosurgery, University of Freiburg Medical Center, Freiburg, Germany; [b] Institute for Signal Processing, University of Luebeck, Luebeck, Germany; [c]College of Medicine, University of Diyala, Diyala, Iraq

ABSTRACT

Differential near infrared sensors recently sparked a growing interest as a promising measuring modality for brain computer interfacing. In our study we present the design and characterization of novel, differential functional NIRS sensors, intended to record hemodynamic changes of the human motor cortex in the hand-area during motor imagery tasks.

We report on the spatial characterization of a portable, multi-channel NIRS system with one module consisting of two central light emitting diodes (LED) (770 nm and 850 nm) and four symmetric pairs of radially aligned photodiodes (PD) resembling a plus symbol. The other sensor module features four similar, differential light paths crossing in the center of a star. Characterization was performed on a concentric, double beaker phantom, featuring a PBS/intralipid/blood mixture (97/1/2%). In extension of previous work, the inner, oxygenated beaker was covered by neoprene sleeves with holes of various sizes, thus giving an estimate on the spatial limits of the NIRS sensor's measurement volume.

The star shaped sensor module formed a diffuse focus of approximately 3 cm in diameter at 1.4 cm depth, whereas the plus shaped arrangement suggested a concentric ring of four separate regions of interest, overall larger than 6 cm. The systems measurement sensitivity could be improved by removing ambient light from the sensing photodiodes by optical filtering.

Altogether, we conclude that both our novel fNIRS design as well as its electronics perform well in the double-layered oxygenation phantom and are thus suitable for in-vivo testing.

Keywords: Dynamic layered tissue phantom, multichannel NIRS system, fNIRS sensor

* Contact: rand.almajidy@klinikum.uni-freiburg.de

1. INTRODUCTION

Several attempts to use the Near Infrared Spectroscopy (NIRS) to monitor changes in brain activity and even Brain-Computer Interfacing have been reported[1, 2]. NIRS features a promising measurement modality[3, 4] in spite of its known limitations[5]. To overcome these limitations NIRS sensors and systems are designed using phantoms made from synthetic materials in order to validate the design prior to use in humans[6]. Some research groups have used tissue phantoms consisting of intralipid and dye displaying a refractive index similar to that of a human infant's head[7]. Others have used multilayered phantoms to mimic scalp and skull optical properties using layers of biological fluid, which mimics the brain's optical properties and exhibit changes during blood oxygen level alteration[8]. Some tissue phantoms even contain multiple, small flexible tubes filled with blood to mimic tissue or brain vasculature[9, 10].

2. METHODOLOGY

NIRS experiments were carried out using a custom-built, multichannel system. The system was connected to a PC via a Beagle Bone (dual core, open embedded developer system) board as presented in Figure 1a. The recording sensor frontend was designed in two different forms, either as a *star* sensor or as a *plus* sensor (see Fig. 1b left and right, resp.). Data collected by the star sensor originated from four intersecting, measuring channels (two light sources 770nm and 850nm in line with two receivers). The plus sensor had only one pair of light sources in the center and two receivers on each arm.

Design and Performance Validation of Phantoms Used in Conjunction with Optical Measurement of Tissue VI, edited by Robert J. Nordstrom, Jean-Pierre Bouchard, David W. Allen, Proc. of SPIE Vol. 8945, 894504

When using the star sensor, each of the four channels' LEDs was turned on sequentially to prevent cross talk between the adjacent channels. The electronic setup is described in detail elsewhere[11]. The plus sensor's photodiode receivers can be turned on simultaneously since all four channels share the same LED light source.
We used the modified Beer-Lambert law to calculate changes in HbO_2 and Hb as previously described[12]. Our dynamic brain tissue phantom consists of 44 ml fresh human blood diluted in 2200 ml of Intralipid solution (1% Intralipid in 10x PBS). This solution is filled into two laboratory beakers (1 l and 2 l) and a bottle (1 l). The fluid in both the beakers and the bottle was continuously agitated using magnetic stirrers. The beakers were concentrically aligned during the experiments. The inner beaker functions to simulate blood content within the brain, whereas the outer beaker mimics blood content within scalp and skull. Both inner and outer beakers were separately sealed gas-tight using Parafilm. Both beakers and the bottle were kept isolated from ambient air at room temperature (22-24 °C). Beakers were reliably mounted in their respective relative positions by a custom-made PLA fitting formed by fused deposition modeling with a 3D printer (Makerbot, Replicator2). In order to simulate hemodynamic changes, either oxygen or nitrogen was bubbled through the blood/Intralipid solution at a rate of ca. 1 l/min. Partial deoxygenation was investigated by bubbling N_2 gas for up to 35 minutes[11], re-oxygenation was achieved by bubbling O_2. We maintained the gas seal by releasing pressure from the inner beaker into a gas trap, i.e., another water filled beaker[13]. The whole experimental setup was placed inside a black box to minimize ambient light effects.

2.1. Simulating hemodynamic responses

The blood oxygenation level detection (BOLD) in functional MRI quantifies the brain's response to an increased oxygen demand during a cognitive task[14]. Thus, we monitored the blood oxygenation level change as the main parameter for our BCI scenario, here simulated by the deoxygenation/re-oxygenation of the blood fraction of the Intralipid mix. The setting consists of a beaker filled with the brain tissue phantom fluid in the mixture mentioned above. One channel of the *star* sensor (Figure 1b) is used to measure the oxygenation level change with only one wavelength LED (770 nm) on. During the experiments the phantom was deoxygenated (N_2 bubbling) for 10-35 minutes, followed by an immediate re-oxygenation (O_2 bubbling) for 5 minutes. Gas flow was carefully adjusted such as to avoid excessive foam formation.

2.2. Effects of ambient light on measurements

Great effort was required in our NIRS setup to minimize the influence of ambient light on photodiode readouts, as previously reported[11]. We consequently cross-tested standard photodiodes (Osram BP 104 S) versus photodiodes (Osram BPW34-FA) with in-built filters for visible light on our dynamic brain tissue phantom.

2.3. Sensor design characterization

2.3.1. Estimating the sensors' spatial resolution

As was deduced from previous work[11], the sensors shown in Fig. 1b have an optimal measurement depth greater than or equal to 1.4 cm in physiologically relevant Intralipid concentrations. In order to characterize the spatial extent at this depth, we limited the area of access to the sensors using circular shielding windows while performing deoxygenation/re-oxygenation experiments with the phantom mixture.
The setup consisted of two concentric beakers filled with the aforementioned tissue phantom fluid while gassing either N_2 or O_2 through the inner beaker. Both beakers were fixed concentrically using a 3D-printed PLA base fixing the distance between them to 1 cm. The 1cm distance plus the 4 mm added thickness of both beakers represent the distance (D) between the sensor and the phantom in the inner beaker. The inner beaker of the dynamic brain tissue phantom was covered with black neoprene with two circular windows (see Fig. 2). For characterization purposes the diameter of the windows was varied between 2-6 cm.

2.3.2. Estimating the sensor's sensitive volume

Even though the presentation of circular measurement areas gives an estimate of the sensitive area of the sensor, actual detected photons do not originate in a plane located 1.4 cm distance from the sensor, but from volumes above and below the measurement plane. In order to characterize the volume necessary to elicit a meaningful sensor readout, the measurement depth was greater than or equal to 1.4 cm, but the volume was allowed to vary. For that purpose, two pairs

of translucent airtight PLA chambers (3D printed) were attached to the inside of the concentrically mounted inner beaker (D =1.4 cm) using medical grade silicone rubber (nusil MED-1000). One pair had the volume of 30.4 cm^3 (4 x 4 x 1.9 cm) with a 3 cm diameter circular window in the external side, the other of 17.1 cm^3 (3 x 3 x 1.9 cm) with a 2 cm diameter circular window in the external side (see Fig. 3a). Chambers were connected by silicone rubber tubing (OD = 10 mm, ID = 6 mm) and were filled, together with the outer and the inner beakers with tissue phantom fluid. Both concentric beakers were sealed airtight and left at their original oxygenation level. For deoxygenation/re-oxygenation experiments gases (N_2 or O_2) were bubbled through an external reservoir and the tissue phantom fluid was circulated through the chambers by a peristaltic pump (Control Company mini pump variable flow, 85 ml/min) (Fig 3 b). As before, each NIRS sensor design was mounted concentrically over each chamber on the outer beaker.

2.3.3 Estimating the sensor's sensitivity to pulsation

Preliminary results did not predict the NIRS spatial resolution in the range of large blood vessels. In a final experiment the measurement chambers were replaced with medical-grade, translucent tubing (OD = 7 mm, ID = 6 mm). In order to compensate for the smaller measurement volume the reservoir and the tubes were filled with whole human blood. Inner and outer beakers were concentrically fixed at D = 1.4 and both were filled with tissue phantom fluid, as above. Blood was continuously circulated through the tubing to/from the gassed reservoir using a peristaltic pump. NIRS sensors were fixed on the outer beaker with their centers coinciding with the tubing.

3. RESULTS AND DISCUSSION

3.1. The optimum brain phantom deoxygenation period

The results shown in Figure 4 reflect the high affinity of hemoglobin to oxygen. It takes more than 20 minutes for the hemoglobin oxygenation level to show a considerable drop. There is a rapid increase in the signal after oxygen is bubbled through the phantom.
After verifying the required deoxygenation period, a single beaker brain tissue phantom was used, with the phantom deoxygenated for 35 min then oxygenated for 10 min. The oxy- and deoxy-hemoglobin concentration changes were calculated using the modified Beer-Lambert law as shown in Figure 5.

3.2. Ambient light reduction

The standard PD has higher sensitivity to the 770 nm LED light, while the filtered PD has somewhat higher sensitivity to the 850 nm LED light (see Fig. 6). Since both wavelengths are used in calculating the oxy- and deoxy-hemoglobin concentration changes, the circuit gain was adjusted to compensate. Thus, the overall performance of the standard PD was deemed better suited than the filtered PD.

3.2.1. Validation by limiting the area for the incident and reflected light

Figure 7 shows the results for both the plus and the star sensor used with an inner beaker shielded with circular windows, which allowed partial light passage through it. When the window diameter was 6 cm, the star sensors showed higher sensitivity as compared to the plus sensor. This could be explained by the fact that for the star sensor the entire sensor diameter was less than 6 cm. Thus, all the channels of the LED and PDs were aligned over the window in the black neoprene sleeves, which minimized the shielding effect. The difference in sensitivity was increased when the window diameter was 4 cm.
This can be related to the LEDs location in the star sensors, which are located within the circumference of the sensors. When the black sleeves have larger windows, the star LEDs' NIR light passes easily in the inner beaker and most of the scattered light can reach the PDs, while in the plus sensors the LEDs are located in the center of the sensors. In this way, light passes through the windows but a higher percentage of the scattered light, as compared to the star sensors, is absorbed by the beaker covering before reaching the PD, which in that case was aligned on top of the black sleeves and higher portion of the NIR light is shielded before reaching PDs. When using black sleeves with 2 cm windows, more light from star sensors' LEDs was absorbed before passing through the inner beaker, which leads to less scattered light. As the LEDs in the plus sensors are located in the center, the light passes easily in the inner beaker but a percentage of

the scattered light is absorbed by the black neoprene sleeves before reaching the PDs. This percentage is less than that of the star sensors, which reflected a higher sensitivity. This difference was also relative looking at the concentration scale.

3.2.2. Validation by limiting the volume of phantom with oxygenation level change

The star sensor showed higher sensitivity when PLA chambers surfaces, which faced the sensor had larger windows, which allowed a higher portion of the NIR scattered light to pass through the chamber, rather than the beakers, before reaching the star sensor PDs compared to the plus sensor. With the smaller chamber surface the NIR scattered light passes through the beakers' phantom fluid rather than the chambers for both of the sensors.

3.2.3. Validating the sensitivity to pulsation

The signal in Figure 9 shows the decrease of the PD voltage due to nitrogen gas bubbling in the blood followed by an increase due to oxygen gas bubbling. The oscillations observed in the signal are caused by the blood, which is pulsating at exactly the pump's frequency (upper right). The filtered signal (Fig 9 bottom) was obtained by using a low pass filter with a frequency equal to the pump rotation frequency, which then resembled the signals shown in Figure 4.

4. CONCLUSIONS

A multichannel NIRS system, which uses PDs as a receiving unit rather than fiber optic systems can provide a small-sized and low cost signal source for motor BCI purposes. Thus, several miniaturized NIR systems have been designed[15, 16]. The specifications of the design and the electronics used in the design governs the accuracy of the data collected from the brain, the depth from which the data are collected and the area to be included. Factors such as patient discomfort and light exposure safety limits play important roles in designing the appropriate electronics.

The proper deoxygenation period for each phantom setting is the key factor in crucial in experiments measuring oxygenation level changes in hemoglobin. Increases in oxygenation level can only be detected after deoxygenation of the sample. Our results showed that due to the slow gas flow rate (which is usually the case in similar experiments) and the high hemoglobin affinity to oxygen a deoxygenation period of at least 20 minutes are necessary to observe changes on hemoglobin saturation.

In order to compensate for the background effect Yurtsever et al. subtracted the signal collected when all LEDs are turned off, which can reduce the data acquisition speed[17]. Safaie et al. suggested using black fabric on the back of the sensor[16]. In our experiments we used filtered PDs, which filter the visible light and allow the NIR light. When both filtered and non-filtered PDs are used the results showed that non-filtered PDs possess a higher sensitivity. This is mainly due to the maximum sensitivity range for non-filtered PDs, which can detect light at 770 nm or less. While for filtered PDs the PD sensitivity decreases as light wavelength approaches that of the visible light. In our experiments we found that using a black neoprene layer on the back of the sensor and around the PDs and LEDs to shield the sensors from the ambient light was a quite practical solution as it doesn't affect the flexibility and adding it on both surfaces prevented both the ambient light and direct PD exposure to LED light.

NIR sensor spatial resolution was estimated by limiting either the NIR light path or the phantom volume, which undergoes oxygenation level changes associated with a small area of interest. The sensors, which were aligned in a manner such that the area of interest is midway between the PD and LED (in our experiments the star sensors), demonstrated a higher sensitivity than those in which the light source coincided with the center of the area of interest. These results agree well with a simulated NIR light path through a brain phantom[18]. The only special case occurs when the area of interest is too small in volume or the light path area is too small. Then, when a larger portion of light scatters through it before detected by the PDs as the case of the plus sensor, the changes reflected by the sensor can be higher.

A multiple-tube tissue phantom has been designed to monitor the variations in blood flow as a helpful tool for evaluation of tumor prognosis and therapy[19]. In our hands, we detected an oscillation in the received signal due to the pulsation in the blood tube caused by the peristaltic pump used. The discovery of this oscillation demonstrated that our system is also capable of detecting pulsation in a tissue phantom. This could also be of importance when monitoring the brain activity or brain injuries.

ACKNOWLEDGEMENTS

The authors are grateful to the blood bank of the University Hospital Freiburg for blood samples. This work was

supported by BrainLinks-BrainTools Cluster of Excellence, which is funded by the German Research Foundation (DFG, grant number EXC 1086).

REFERENCES

[1] Gervain, J., Mehler, J., Werker, J. F., Nelson, C. A., Csibra, G., Lloyd-Fox, S., Shukla, M. and Aslin, R. N., "Near-infrared spectroscopy: A report from the McDonnell infant methodology consortium," Dev. Cogn. Neurosci. 1, 22–46 (2011).

[2] Coyle, S. M., Ward, T. E. and Markham, C. M., "Brain–computer interface using a simplified functional near-infrared spectroscopy system," J. Neural Eng. 4(3), 219–226 (2007).

[3] Fazli, S., Mehnert, J., Steinbrink, J., Curio, G., Villringer, A., Müller, K. R. and Blankertz, B., "Enhanced performance by a hybrid NIRS–EEG brain computer interface," Neuroimage 59(1), 519–529 (2012).

[4] Yu, J., Ang, K. K., Guan, C. and Wang, C., "A Multimodal fNIRS and EEG-Based BCI study on motor imagery and passive movement," Proc. 6th Annual International IEEE EMBS Conference on Neural Engineering, San Diego, California, 5-8 (2013).

[5] Strait, M., Canning, C. and Scheutz, M., "Limitations of NIRS-Based BCI for realistic applications in human-computer interaction," Proc. 5th International Brain-Computer Interface Meeting (2013).

[6] Sasai,S. , Homae, F., Watanabe,H. and Taga ,G., "Frequency-specific functional connectivity in the brain during resting state revealed by NIRS," Neuroimage 56(1), 252–257 (2011).

[7] Hebden, J.C., Gibson, A., Yusof, R. M., Everdell, N., Hillman, E. M., Delpy, D. T., Arridge, S. R., Austin, T., Meek, J. H. and Wyatt J. S., "Three-dimensional optical tomography of the premature infant brain," Phys. Med. Biol. 47(23), 4155–4166 (2002).

[8] Wolf, M., Keel, M., Dietz, V., von Siebenthal, K., Bucher, H. U. and Baenziger, O., "The influence of a clear layer on near-infrared spectrophotometry measurements using a liquid neonatal head phantom," Phys. Med. Biol. 44(7), 1743–1753 (1999).

[9] Kurth, C. D., Liu, H., Thayer, W. S. and Chance, B., "A dynamic phantom brain model for near-infrared spectroscopy," Phys. Med. Biol. 40(12), 2079-2092 (1995).

[10] Kashyap, D., Chu, N., Apte, A., Wang, B. P. and Liu, H., "Development of broadband multi-channel NIRS (Near Infrared Spectroscopy) imaging system for quantification of spatial distribution of hemoglobin derivatives," Proc. SPIE 6434, (2007).

[11] Almajidy, R. K. and Hofmann, U. G., "On the design of a multichannel NIRS system to monitor functional brain activity," Proc.16th International Conference on Near Infrared Spectroscopy in La Grande-Motte, France, International Council for Near Infrared Spectroscopy, 335-338 (2013).

[12] Delpy, D. T., Cope, M., van der Zee, P., Arridge, S., Wray, S. and Wyatt, J., "Estimation of optical pathlength through tissue from direct time of flight measurement," Phys. Med. Biol. 33(12), 1433-1442 (1988).

[13] Kashyap D., "Development of a broadband multi-channel NIRS system for quantifying absolute concentrations of hemoglobin derivatives and reduced scattering coefficients," PhD thesis, University of Texas, Arlington, 93-96 (2007).

[14] Logothetis, N., Pauls, J., Augath, M., Trinath, T. and Oeltermann, A., "Neurophysiological investigation of the basis of the fMRI signal," Nature 412(6843), 150-157 (2001).

[15] Muehlemann, T., Haensse, D. and Wolf, M., "Wireless miniaturized in-vivo near infrared imaging," Opt. Express 16(14), 10323-10330 (2008).

[16] Safaie, J., Grebe, R., Moghaddam, H. A. and Wallois, F., "Wireless Distributed Acquisition System For Near Infrared Spectroscopy-WDA-NIRS," J. Innovative Optical Health Sciences, 6 (3), 1350019-1-1350019-15 (2013).

[17] Yurtsever, G., Ayaz, H., Kepics, F., Onaral, B. and Pourrezaei, K., "Wireless, Continuous Wave near Infrared Spectroscopy System for Monitoring Brain Activity," Philadelphia, PA: Drexel University (2006).

[18] Okada, E., "The effect of superficial tissue of the head on spatial sensitivity profiles for near infrared spectroscopy and imaging," Optical Review 7(5), 375-382 (2000).

[19] Ranga, R., Kashyap, D., Behbehani, K. and Liu, H., "An in vitro hemodynamic tissue model to study the variations in flow using near infrared spectroscopy," Proc. SPIE 5693, 366-371 (2005).

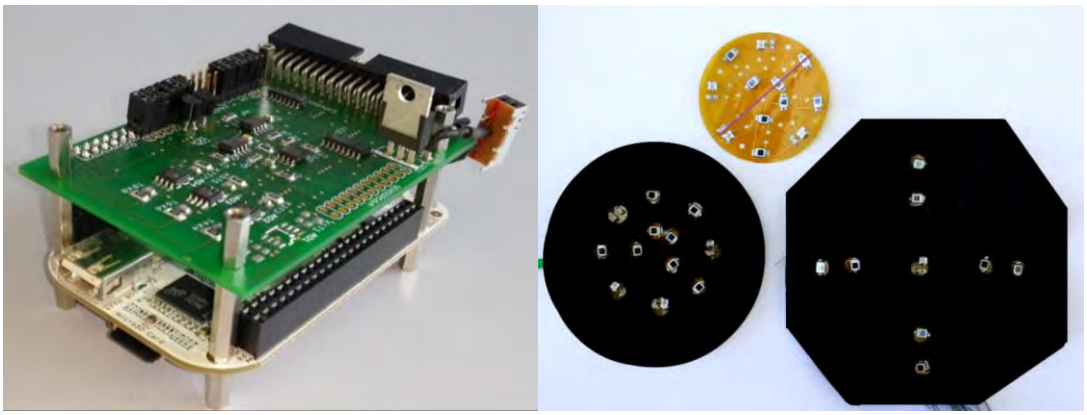

(a) (b)

Figure 1. Multichannel NIRS system: (a) Control circuit mounted to a Beagle Bone board and (b) the *star* (left) and the *plus* (right) multichannel sensors. (top) electronic interconnect for the *star* sensor (PCB), the line designates a single channel.

Figure 2. Artistic rendering of the two concentric beakers and a neoprene sleeve with circular windows around the inner beaker. *Star* (left) and *plus* (right) sensors are mounted centrally over of each of these windows.

(a) (b)

Figure 3. (a) Artistic rendering of the inner beaker and one chamber attached to its inner surface. (b) An airtight bottle acts as a reservoir and contains the agitated and gassed brain phantom fluid. In a final experiment, the chamber is completely replaced by a silicone tube.

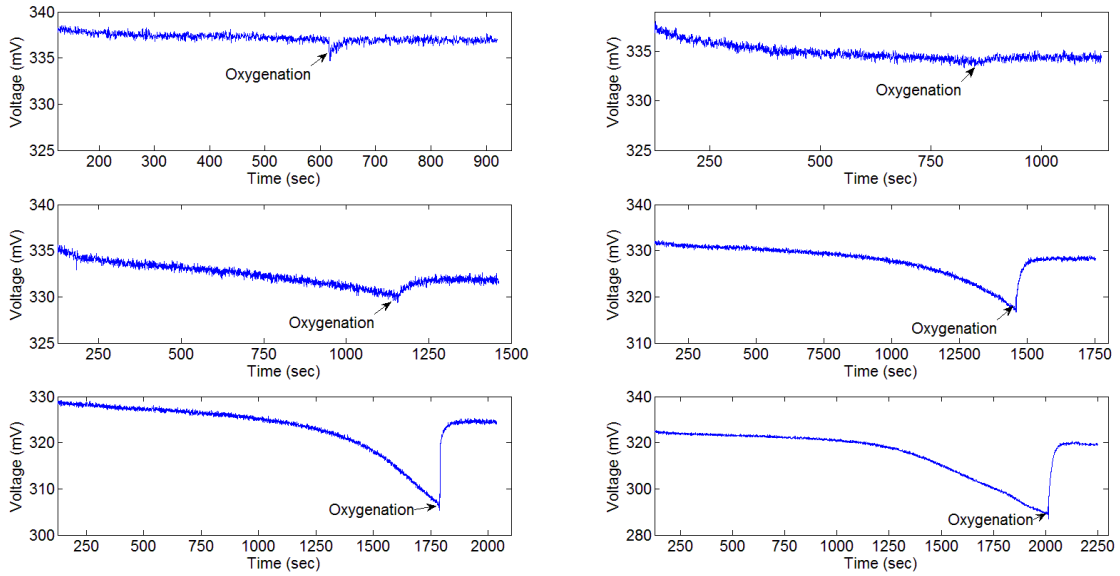

Figure 4. The change in PD voltage drop associated with nitrogen bubbling period increase.

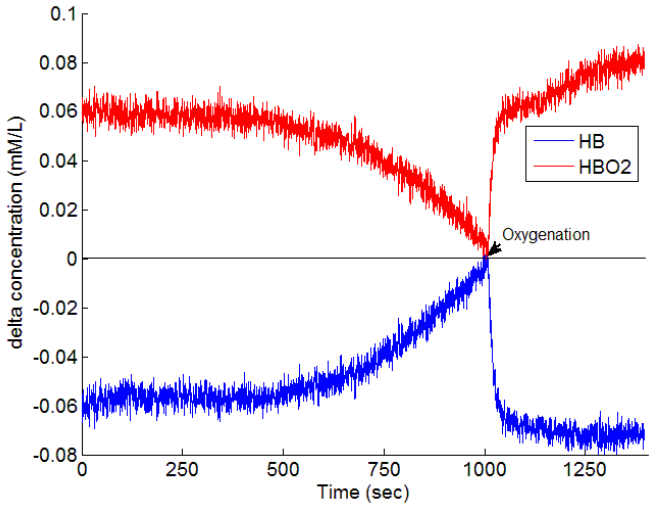

Figure 5. The concentration changes of oxygenated and deoxygenated hemoglobin when bubbling nitrogen then oxygen in the brain tissue phantom.

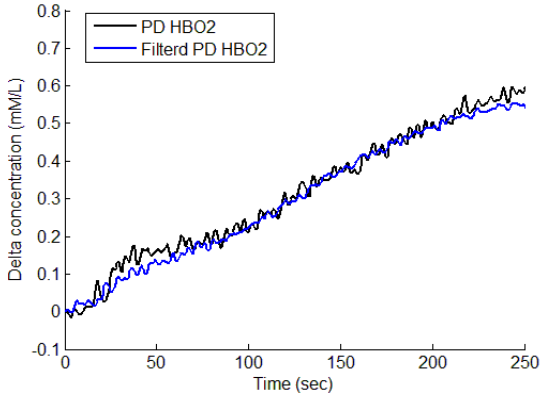

Figure 6. The difference in oxygenated hemoglobin using sensors equipped with filtered and standard PDs.

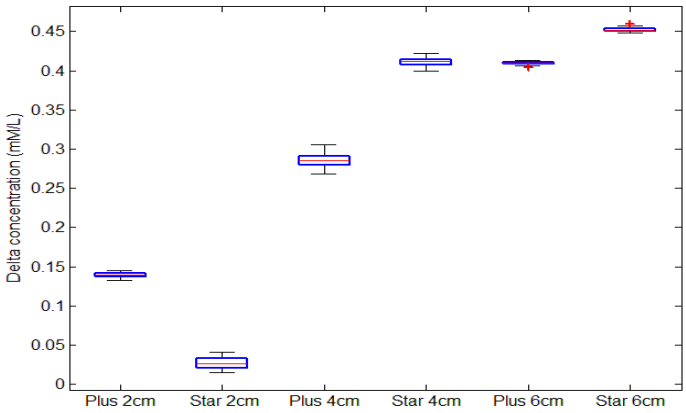

Figure 7. The box plot of deoxygenated hemoglobin concentration in the phantom, when using a black neoprene sleeves with windows to allow a portion of the NIR light to pass through the inner beaker (which is used to simulate the brain) before scattering back to the surface.

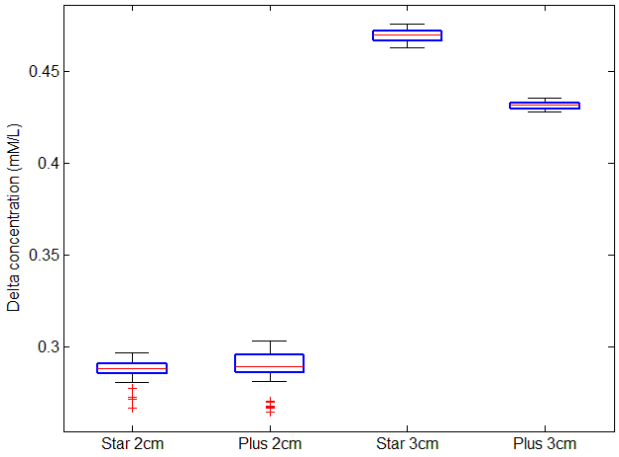

Figure 8. The box plot of deoxygenated hemoglobin concentration in the phantom, when using translucent PLA chambers with different volumes to allow a portion of the NIR light to pass through the inner beaker (which is used to simulate the brain) before scattering back to the surface.

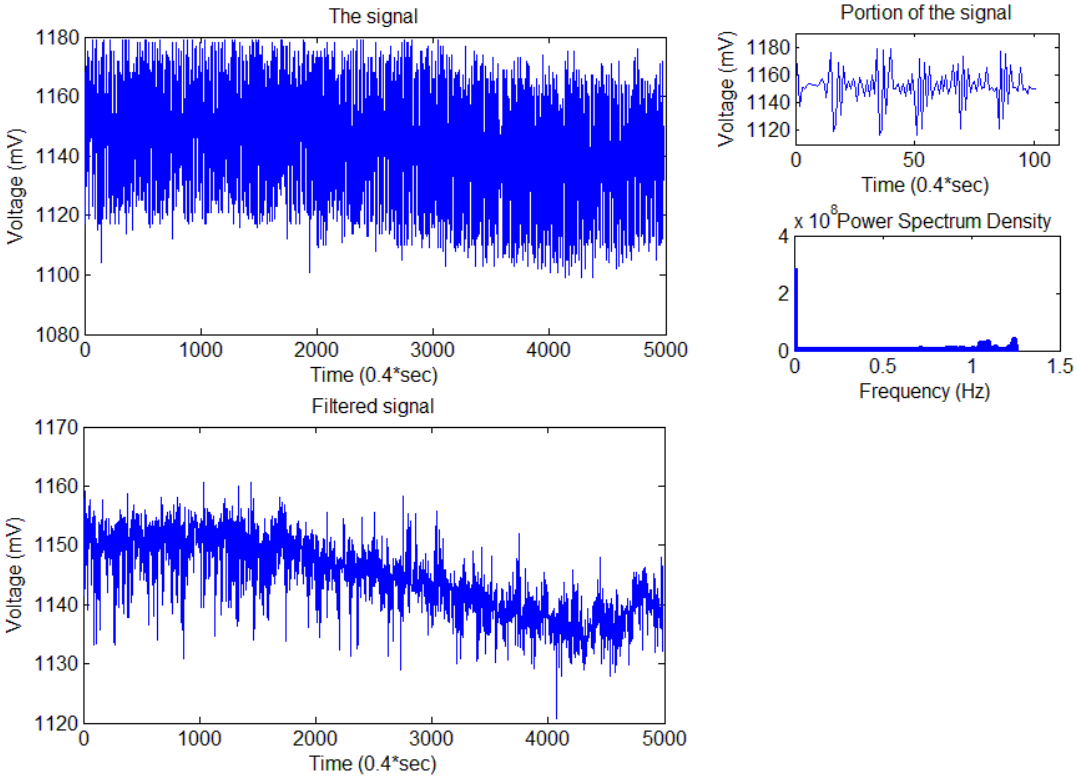

Figure 9. The change in PD voltage when using 770nm LED during deoxygenation followed by oxygenation of the blood. The top plot shows the signal and the oscillation due to the pump. The bottom plot shows the signal after filtering the pump frequency. A portion of the top plot is expanded and shown in the upper right. The power spectrum density is shown in lower right.